Exact Treatment of the Dispersion and Beam Interaction Impedance of a Thin Tape Helix Surrounded by a Radially Stratified Dielectric

D. Chernin
Science Applications International Corporation
McLean, VA 22102

T.M. Antonsen, Jr.
Institute for Plasma Research
University of Maryland
College Park, MD 20742

B. Levush
Naval Research Laboratory
Washington, DC 20875

November 23, 1998

Abstract

An exact dispersion relation is obtained for electromagnetic waves propagating on a thin metallic tape helix of arbitrary width, supported by a radially stratified dielectric layer and enclosed by a metallic shell.   By expanding the surface currents on the tape in a series of Chebyshev polynomials, the unquantifiable assumptions made in all previously published analyses of the tape helix regarding the forms of the surface current on the tape, or the electric fields at the radius of the tape, are avoided.   The power flow and interaction impedance are exactly computed.   The dispersion relation is solved numerically for slow waves and the resulting phase velocity and interaction impedance are compared to those computed using the frequently made assumptions of constant current along the tape and zero current across the tape.   It is found that for wide tapes significant errors are made in both the phase velocity and interaction impedance when neglecting the transverse variation of the longitudinal current and neglecting the transverse current.   For narrow tapes, the two approaches agree to good accuracy. Plots of the surface currents for wide and narrow tapes are presented.   The longitudinal current shows a significant variation across the tape.   An example is given showing the existence of an optimum tape width, at which the on-axis interaction impedance is maximized.   It is separately shown how an approximate, but useful model of metallic vanes may be incorporated in the analysis by the modification of certain boundary conditions.   In all cases, computations of phase velocity and impedance across a wide frequency band take well under a minute on a modern workstation.

1. Introduction

The characterization of the electromagnetic waves supported by a metallic helix has been the subject of extensive investigations, beginning, apparently, with an approximate treatment by Pocklington[1], who analyzed waves supported by a thin wire helix. It was not until the invention of the helix traveling wave tube by Kompfner[2], however, and its subsequent analysis by Pierce[3], that interest in the details of the slow wave electromagnetic modes of a helix greatly increased. The first comprehensive analytical treatment of the problem was presented by Sensiper in his doctoral thesis[4], some of which was abstracted in a later review article[5], where many references up to 1955 may be found. Sensiper discussed both the so-called sheath model of the helix, in which currents are constrained to flow in helical paths on a cylindrical wall, as well as a finite width tape model, which contains the effects of spatial harmonics absent from the sheath model. In both cases, Sensiper's analysis applies to an unsupported helix in free space. The effects of a supporting dielectric layer were investigated by Tien[6] and by McMurtry[7], who also considered the effect of a surrounding metal tube. A good summary appears in Watkins[8]. More recently, Freund, et. al.[9] computed the dispersive properties of a tape helix surrounded by a cylindrical metal waveguide in connection with their analysis of the linearized beam-circuit interaction in a TWT. Ghosh, et. al.[10] presented an analysis of the tape helix surrounded by a stratified, multi-layer dielectric support.

All previous work on the tape helix of which the present authors are aware have included some simplifying assumptions about the surface current density distribution on the tape and/or have enforced the boundary conditions on the electric field at the tape in an approximate way. The 'narrow tape' assumptions seem to be the most common. These are that (1) the current flows only along, not across, the tape, (2) the current density along the tape is constant across the width of the tape, and (3) $E_\parallel = 0$ along the tape centerline. Sometimes assumption (3) is replaced by the condition that the average of $E_\parallel$ across the tape vanishes, though this gives results very similar to (3), for narrow tapes. Sensiper, apparently uniquely, separately treated the wide tape (narrow gap) case, by assuming that $E_\parallel$ vanished everywhere at the radius of the tape, the electric field in the gap was constant, and the transverse current at the center of the gap vanished, though, again, his analysis applied only to an unsupported helix in free space.

Freund, et. al. and Ghosh, et. al. in particular applied (1), (2), and (3). These approximations are expected to be good for narrow tapes. However, they are not essential, nor are they necessarily physically reasonable. In particular, assumption (2) omits the expected square root singularity of the parallel current density at the tape edges, present even for narrow tapes. In the present report it is shown how these common assumptions may be eliminated and a formally exact dispersion relation obtained for the (infinitely radially thin) metal tape helix supported by a radially stratified dielectric layer, surrounded by a cylindrical metal waveguide. An exact expression for the power flow, from which the interaction impedance may be obtained, is also given.

The assumption of an infinitely thin tape presents a question of how the predictions of the theory presented here could be compared with experimental measurements on real, finite thickness tapes. In the usual case, in which the skin depth is small compared to the actual tape thickness, slightly different currents flow on the inner and outer surfaces of the tape. This could be taken approximately into account, for example, by treating two helical surface currents separated by a vacuum gap representing the tape thickness, but no attempt to do this is made in the present paper. Here we present the first exact treatment of a single thin tape. Generalizations of the analysis used here to treat multiple tapes, even counter-wound tapes, are straightforward.

This paper is organized as follows: Section 2, below, presents the derivation of the dispersion relation and power flow for the case of a single dielectric layer between the helix and the outer wall. The formulation is such that it is easily generalized to the case of an arbitrary number of dielectric layers; this is done in Section 3, where a simple matrix approach is used to propagate the fields across the multiple layers. Section 4 presents some numerical examples, demonstrating the breakdown of the narrow tape assumptions. It is also shown that there is a maximum in the interaction impedance as a function of tape width, the maximum occurring at a value at which neither the narrow tape nor narrow gap assumptions is expected to be valid.

2. Single Dielectric Supporting Layer

We begin by considering electromagnetic waves supported by a tape helix centered inside a perfectly conducting circular cylinder with a single azimuthally uniform dielectric lining, as shown in Figure 1. The radius of the helix is a, its width is w and its period or pitch in the axial (z) direction is p. The tape is taken to be infinitely thin in the radial direction. The radius of the

enclosing cylinder is b. The pitch angle of the helix, ψ, is defined by $cot\,\psi \equiv 2\pi a/p$. Cylindrical coordinates (r, θ, z) are used, as shown in the figure.

The interior of the helix ($0 \le r < a$; region 1) is taken to be vacuum. The region between the helix and the outer wall ($a < r < b$; region 2) is filled uniformly with a single layer of dielectric material of permittivity $\varepsilon^{(2)} \equiv \varepsilon_r^{(2)} \varepsilon_o$ where ε_o is the permittivity of free space. Superscripts $^{(1)}$ and $^{(2)}$ are used here and below to denote regions 1 and 2. The general case in which the dielectric region between the helix and outer wall is radially stratified into multiple layers with different dielectric constants is treated in the next section.

(a)

(b)
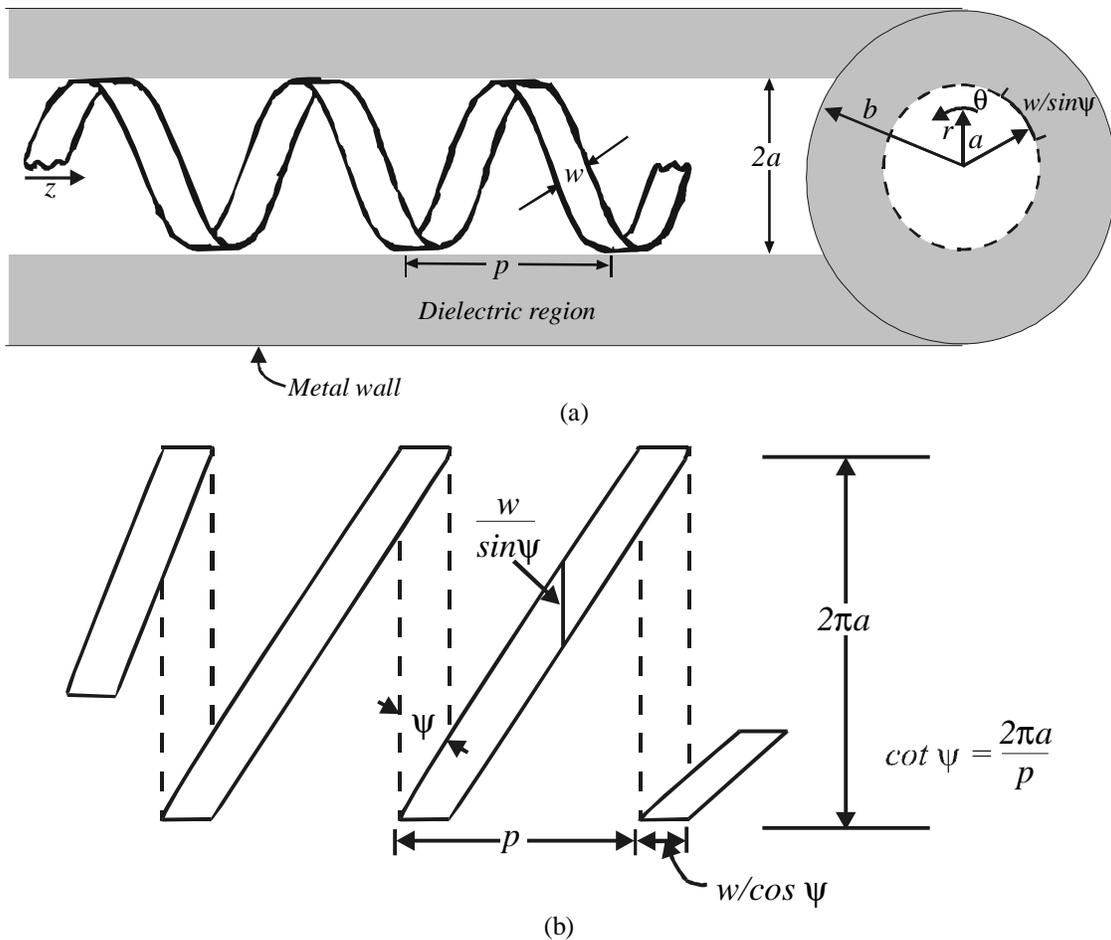
Figure 1.   Right-handed tape helix surrounded by a single dielectric layer enclosed in a cylindrical metal waveguide.   The helix radius is a, its width is w, and its pitch is p.   The waveguide radius is b. The developed helix (cut along z and unrolled) is shown in (b).   The tape cuts a plane of constant z in a width $w/sin\,\psi$ as shown in (b), where $cot\,\psi \equiv 2\pi a/p$.

To begin, we need only Faraday's and Ampere's laws which, in *mks* units, are:

$$\vec{\nabla} \times \vec{E} = -j\omega\vec{B} \tag{1}$$

$$\vec{\nabla} \times \vec{H} = j\omega\vec{D} + \vec{J} \tag{2}$$

where $\vec{B} = \mu_o\vec{H}$; $\vec{D} = \varepsilon\,\vec{E}$ and a time dependence $\sim exp(j\omega t)$ has been assumed. The current $\vec{J}$ is confined to the (infinitely thin) tape and to the wall of the enclosing cylinder. For $r<b$, we write

$$\vec{J}(r,\theta,z) = \delta(r-a)[J_\theta(\theta,z)\hat{\theta} + J_z(\theta,z)\hat{z}] \tag{3}$$

where $\vec{J}(\theta,z)$ is the surface current density at $r = a$, and $\delta(r-a)$ is the Dirac delta function.

We take all field and current components to be of the ("Floquet") form,

$$F(r,\theta,z) = e^{-j\beta z}\sum_{n=-\infty}^{\infty} F_n(r)e^{jn(\theta-k_H z)} \tag{4}$$

where $k_H=2\pi/p$. The helix period p is positive for a right-handed helix and negative for a left-handed helix. βp is the phase shift per period. The propagation factor β is an as yet unknown function of frequency, ω, and the other parameters of the problem.

Now, it follows from Eqs.(1) and (2) that E_{zn} and H_{zn} separately satisfy

$$\left[\frac{1}{r}\frac{\partial}{\partial r}r\frac{\partial}{\partial r} - (\gamma_n^{(i)2} + \frac{n^2}{r^2})\right]F_n^{(i)} = 0 \tag{5}$$

in each region ($i=1,2$), where $F_n^{(i)}$ denotes either $E_{zn}^{(i)}$ or $H_{zn}^{(i)}$,

$$\gamma_n^{(i)2} \equiv \beta_n^2 - \varepsilon_r^{(i)}\frac{\omega^2}{c^2}, \tag{6}$$

is the square of the radial propagation factor in region *(i),* and

$$\beta_n \equiv \beta + nk_H \tag{7}$$

is the axial propagation factor in all regions.

Equations (1) and (2) may also be used to express the r- and θ- components of the fields in terms of the z-components and their radial derivatives as follows:

$$\gamma_n^{(i)2} E_{rn}^{(i)} = j\beta_n \frac{\partial}{\partial r} E_{zn}^{(i)} - \frac{\omega n}{r} \mu_o H_{zn}^{(i)} \tag{8a}$$

$$\gamma_n^{(i)2} E_{\theta n}^{(i)} = \frac{-n\beta_n}{r} E_{zn}^{(i)} - j\omega\mu_o \frac{\partial}{\partial r} H_{zn}^{(i)} \tag{8b}$$

$$\gamma_n^{(i)2} H_{rn}^{(i)} = \varepsilon^{(i)} \omega \frac{n}{r} E_{zn}^{(i)} + j\beta_n \frac{\partial}{\partial r} H_{zn}^{(i)} \tag{8c}$$

$$\gamma_n^{(i)2} H_{\theta n}^{(i)} = j\varepsilon^{(i)} \omega \frac{\partial}{\partial r} E_{zn}^{(i)} - \frac{n\beta_n}{r} H_{zn}^{(i)} \tag{8d}$$

where, again, these equations hold separately in regions 1 and 2.

The goal of the calculation that follows is to express the components of $\vec{E}$ parallel to the helix in terms of the helix surface currents. Requiring those components of $\vec{E}$ to vanish on the (perfectly conducting) helix surface will then give a homogeneous equation for the components of the surface currents. The condition for existence of a non-trivial solution of that equation gives the dispersion relation, relating the propagation constant β to ω (and to the other parameters of the problem). The resulting currents can then be used to compute all field components.

Equations (2) and (3) give the jump conditions on $\vec{H}$, at the helix ($r=a$):

$$H_{zn}^{(2)}(a) - H_{zn}^{(1)}(a) = -\mathsf{J}_{\theta n} \tag{9a}$$

$$H_{\theta n}^{(2)}(a) - H_{\theta n}^{(1)}(a) = \mathsf{J}_{zn}. \tag{9b}$$

Evaluating Eqs. (8b, d) at $r=a$, defining the dimensionless logarithmic derivatives

$$l_{En}^{(i)} \equiv \frac{1}{\gamma_n^{(i)} E_{zn}^{(i)}} \frac{\partial E_{zn}^{(i)}}{\partial r}\Big|_{r \to a} \tag{10a}$$

$$l_{Hn}^{(i)} \equiv \frac{1}{\gamma_n^{(i)} H_{zn}^{(i)}} \frac{\partial H_{zn}^{(i)}}{\partial r}\Big|_{r \to a} \tag{10b}$$

and solving for $H_{\theta n}^{(i)}$ and $H_{zn}^{(i)}$ in terms of $E_{\theta n}^{(i)}$ and $E_{zn}^{(i)}$ gives

$$\begin{pmatrix} H_{\theta n}^{(i)} \\ H_{zn}^{(i)} \end{pmatrix} = Y_n^{(i)} \begin{pmatrix} E_{\theta n}^{(i)} \\ E_{zn}^{(i)} \end{pmatrix} \tag{11}$$

where 2×2 admittance matrices $Y_n^{(i)}$ have been defined as

$$Y_n^{(i)} = \frac{-j\beta_n c}{\zeta_o \gamma_n^{(i)} l_{Hn}^{(i)} \omega a} \begin{pmatrix} n & \dfrac{n^2 \beta_n}{\gamma_n^{(i)2} a} - \varepsilon_r^{(i)} \dfrac{\omega^2}{c^2} \dfrac{a}{\beta_n} l_{Hn}^{(i)} l_{En}^{(i)} \\ -\dfrac{\gamma_n^{(i)2} a}{\beta_n} & -n \end{pmatrix}, \tag{12}$$

where $\zeta_0 \equiv \mu_0 c \approx 377\Omega$ is the impedance of free space.

The logarithmic derivatives defined in Eqs. (10a, b) and appearing in Eq. (12) are given by the solutions of Eq.(5). The interior of the helix (Region 1) is assumed to be vacuum. It follows that

$$l_{En}^{(1)} = l_{Hn}^{(1)} = \frac{I_n'(x_n^{(1)})}{I_n(x_n^{(1)})} \tag{13}$$

where I_n is the modified Bessel function of the first kind, $x_n^{(1)} \equiv \gamma_n^{(1)} a$, a is the helix radius, and a prime mark denotes differentiation with respect to the argument of the modified Bessel function. Similarly, applying Eq.(5) in Region 2 and enforcing the appropriate boundary conditions at the outer wall gives

$$l_{En}^{(2)} = \frac{I_n'(x_n^{(2)}) K_n(y_n^{(2)}) - I_n(y_n^{(2)}) K_n'(x_n^{(2)})}{I_n(x_n^{(2)}) K_n(y_n^{(2)}) - I_n(y_n^{(2)}) K_n(x_n^{(2)})} \tag{14a}$$

$$l_{Hn}^{(2)} = \frac{I_n'(x_n^{(2)}) K_n'(y_n^{(2)}) - I_n'(y_n^{(2)}) K_n'(x_n^{(2)})}{I_n(x_n^{(2)}) K_n'(y_n^{(2)}) - I_n'(y_n^{(2)}) K_n(x_n^{(2)})} \tag{14b}$$

where $x_n^{(2)} \equiv \gamma_n^{(2)} a$, $y_n^{(2)} \equiv \gamma_n^{(2)} b$, b is the wall radius, and K_n is the modified Bessel function of the second kind.

Defining now the jump in the magnetic field $\Delta H = H^{(2)}(a) - H^{(1)}(a)$ at the helix radius, Eqs. (9a,b) and (11) give

$$\begin{pmatrix} \Delta H_{\theta n} \\ \Delta H_{zn} \end{pmatrix} = \left(Y_n^{(2)} - Y_n^{(1)} \right) \begin{pmatrix} E_{\theta n} \\ E_{zn} \end{pmatrix} = \begin{pmatrix} J_{zn} \\ -J_{\theta n} \end{pmatrix}, \tag{15}$$

where the superscripts on $E_{\theta n}$ and E_{zn} have been dropped, since these fields are continuous at $r = a$. Solving for $E_{\theta n}$ and E_{zn} in terms of the surface currents on the helix gives the basic result

$$\begin{pmatrix} E_{\theta n} \\ E_{zn} \end{pmatrix} = Z_n \begin{pmatrix} J_{zn} \\ - J_{\theta n} \end{pmatrix} \tag{16}$$

where the 2×2 impedance matrix Z_n has been defined as

$$Z_n \equiv \left(Y_n^{(2)} - Y_n^{(1)} \right)^{-1}. \tag{17}$$

The total E field at the tape radius ($r=a$) is then

$$\begin{pmatrix} E_\theta \\ E_z \end{pmatrix}(\theta, z) = \frac{1}{2\pi} \sum_n Z_n \int_0^{2\pi} d\theta' e^{jn(\theta-\theta')} \begin{pmatrix} J_z \\ -J_\theta \end{pmatrix}(\theta', z). \tag{18}$$

In order to apply the boundary conditions $E_\theta = E_z = 0$ on the tape itself, it is convenient to define surface coordinates on the cylinder $r=a$ as

$$\xi \equiv a\theta \cos\psi + z \sin\psi \tag{19a}$$

$$\eta \equiv -a\theta \sin\psi + z \cos\psi \tag{19b}$$

where the helix pitch angle ψ is defined by

$$\cot\psi = k_H a. \tag{20}$$

The limiting cases ($k_H \to 0$, $\psi \to \pi/2$, $\xi \to z$, $\eta \to -a\theta$) and ($k_H \to \infty$, $\psi \to 0$, $\xi \to a\theta$, $\eta \to z$) correspond to a strip along z and a very tightly wound helix, respectively. In the general case, the ξ- direction is measured along the tape ($-\infty < \xi < \infty$) and the η- direction is measured across the tape ($0 < \eta < w$) where w is the tape width. For any vector (V_θ, V_z), the transformation to (ξ, η) coordinates is given by a rotation

$$\begin{pmatrix} V_\xi \\ V_\eta \end{pmatrix} = \begin{pmatrix} \cos\psi & \sin\psi \\ -\sin\psi & \cos\psi \end{pmatrix} \begin{pmatrix} V_\theta \\ V_z \end{pmatrix} \equiv R \begin{pmatrix} V_\theta \\ V_z \end{pmatrix}, \tag{21}$$

which defines the rotation matrix R. Performing this change of variables in Eq. (18) yields

$$\begin{pmatrix} E_\xi \\ E_\eta \end{pmatrix}(\xi, \eta) = \frac{1}{2\pi a \sin\psi} \sum_n \tilde{Z}_n \int_o^w d\eta' e^{-jn(\eta-\eta')/a\sin\psi} \begin{pmatrix} J_\xi \\ J_\eta \end{pmatrix}(\xi + \cot\psi(\eta - \eta'), \eta') \tag{22}$$

where

$$\tilde{Z}_n \equiv RZ_n \begin{pmatrix} 0 & 1 \\ -1 & 0 \end{pmatrix} R^{-1}. \tag{23}$$

The boundary condition at the tape is $E_\xi(\xi,\eta) = E_\eta(\xi,\eta) = 0$ for $-\infty < \xi < \infty$ and $0 < \eta < w$. In order

to apply this boundary condition, it is convenient to take a Fourier transform in ξ. Writing

$$F(\xi,\eta) = e^{-j\kappa\xi} F_\kappa(\eta) \tag{24}$$

for any F, where κ is the wave number in the ξ-direction, Eq. (22) becomes

$$e^{-j\kappa\xi} \begin{pmatrix} E_{\xi\kappa} \\ E_{\eta\kappa} \end{pmatrix} = e^{-j\kappa(\xi+\eta\cot\psi)} \frac{1}{2\pi a \sin\psi} \sum_n e^{-jn\eta/a\sin\psi} \int_o^w d\eta' e^{jn'\left[\frac{n}{a\sin\psi}+\kappa\cot\psi\right]} \tilde{Z}_n \begin{pmatrix} J_{\xi\kappa} \\ J_{\eta\kappa} \end{pmatrix} \tag{25}$$

Noting that

$$\xi + \eta\cot\psi = \frac{z}{\sin\psi} \tag{26a}$$

$$-\frac{\eta}{a\sin\psi} = \theta - k_H z \tag{26b}$$

it follows that Eq. (25) has the form of Eq. (4) if we identify

$$\kappa \equiv \beta \sin\psi \tag{27}$$

as the wavenumber along the tape. It remains then only to satisfy the condition

$$\begin{pmatrix} E_{\xi\kappa} \\ E_{\eta\kappa} \end{pmatrix} = 0 \text{ in } 0 < \eta < w. \tag{28}$$

Using Eq. (25), this condition is written

$$\begin{pmatrix} E_\xi(s) \\ E_\eta(s) \end{pmatrix} = \frac{(w/2)}{2\pi a \sin\psi} \sum_n \int_{-1}^1 ds' e^{-j\alpha_n(s-s')} \tilde{Z}_n \begin{pmatrix} J_\xi(s') \\ J_\eta(s') \end{pmatrix} = 0 \tag{29}$$

in $-1 < s < 1$ where

$$\alpha_n \equiv \frac{w}{2}\left[\frac{n}{a\sin\psi} + \beta\cos\psi\right] = \overline{w}\left(n\pi + \frac{\phi}{2}\cos^2\psi\right), \tag{30}$$

$$\overline{w} \equiv w/(p\cos\psi) \tag{31}$$

9

is the dimensionless tape width $(0 < \overline{w} < 1)$, $\phi \equiv \beta p$ is the phase shift per period, and we have changed variables from η to s,

$$s \equiv 2\frac{\eta}{w} - 1,$$

(32)

so that the range of s is $[-1,1]$ across the tape. Note that $s = +1$ is the downstream edge of the tape, that is, a point moving with the phase velocity of the wave passes $s = -1$ first, then $s = +1$. The subscript κ has been dropped in Eq. (29), and in the following.

Eq. (29) is a homogeneous integral equation for the functions $J_\xi(s)$ and $J_\eta(s)$. The condition for the existence of a non-trivial solution of Eq. (29) is the dispersion relation we seek. One approach to obtaining this dispersion relation is to expand $J_\xi(s)$ and $J_\eta(s)$ in a complete set of functions on the interval $(-1,1)$ and to project out the coefficients of each element of the set from Eq. (29), setting each to zero. The result is a homogeneous matrix equation. Setting the determinant of the coefficient matrix to zero gives the dispersion relation. Following this approach, we write

$$J_\xi(s) = \frac{1}{(1-s^2)^{1/2}} \sum_{l=0}^{\infty} J_{\xi l} T_l(s)$$

(33a)

$$J_\eta(s) = (1-s^2)^{1/2} \sum_{l=0}^{\infty} J_{\eta l} U_l(s)$$

(33b)

where $T_l(s)$ and $U_l(s)$ are the Chebyshev polynomials of the first and second kinds[11] and the expansions have been chosen so that the currents have the expected behavior at the edges of the tape, $s=\pm 1$. Useful integrals involving the Chebyshev polynomials are

$$\int_{-1}^{1} ds \frac{T_l(s) T_m(s)}{(1-s^2)^{1/2}} = \begin{cases} 0 & l \neq m \\ \pi & l = m = 0 \\ \pi/2 & l = m \neq 0 \end{cases}$$

(34a)

$$\int_{-1}^{1} ds (1-s^2)^{1/2} U_l(s) U_m(s) = \begin{cases} 0 & l \neq m \\ \pi/2 & l = m \end{cases}$$

(34b)

$$\int_{-1}^{1} ds\, e^{j\alpha s} \frac{T_l(s)}{(1-s^2)^{1/2}} = \pi\, j^l J_l(\alpha) \tag{34c}$$

$$\int_{-1}^{1} ds\, e^{j\alpha s} (1-s^2)^{1/2} U_l(s) = \pi\, j^l \frac{l+1}{\alpha} J_{l+1}(\alpha) \tag{34d}$$

where, in (34c, d), J_l is the Bessel function of the first kind.

Substituting (33a, b) in (29) and operating by the matrix operator

$$\begin{pmatrix} \displaystyle\int_{-1}^{1} ds\, \frac{T_l(s)}{(1-s^2)^{1/2}} & 0 \\[2ex] 0 & \displaystyle\int_{-1}^{1} ds(1-s^2)^{1/2} U_l(s) \end{pmatrix} \bullet \tag{35}$$

gives

$$\mathsf{M}_{ll'}\begin{pmatrix} \mathsf{J}_{\xi l'} \\ \mathsf{J}_{nl'} \end{pmatrix} = 0 \tag{36}$$

where a sum from $0\rightarrow\infty$ on l' is understood and the doubly infinite set of 2x2 matrices $\mathsf{M}_{ll'}$, $(l,\ l' =0,1,2,\dots\ \infty)$ is given by

$$M_{ll'} = (-1)^l\, j^{l+l'} \sum_{n=-\infty}^{\infty} \begin{pmatrix} J_l(\alpha_n) & 0 \\ 0 & \dfrac{l+1}{\alpha_n} J_{l+1}(\alpha_n) \end{pmatrix} \widetilde{Z}_n \begin{pmatrix} J_{l'}(\alpha_n) & 0 \\ 0 & \dfrac{l'+1}{\alpha_n} J_{l'+1}(\alpha_n) \end{pmatrix}. \tag{37}$$

If we expand Eq.(34)

$$\begin{pmatrix} M_{00} & M_{01} & M_{02} & \dots \\ M_{10} & M_{11} & M_{12} & \dots \\ M_{20} & M_{21} & M_{22} & \dots \\ \dots & \dots & \dots & \dots \end{pmatrix} \begin{pmatrix} \mathsf{J}_{\xi 0} \\ \mathsf{J}_{\eta 0} \\ \mathsf{J}_{\xi 1} \\ \mathsf{J}_{\eta 1} \\ \dots \end{pmatrix} \equiv MJ \equiv 0. \tag{38}$$

The complete dispersion relation is then

$$\det\mathsf{M}=0 \tag{39}$$

11

where M is the infinite matrix in Eq. (38).

Eq. (39) is (formally) exact. Its solution includes all waves (both fast and slow) that can be supported by the helix. The only implicit assumption is that the currents possess convergent expansions of the form (33a,b).

Note that the elements of M, defined in (37), depend on those of the admittance matrices in region (1) -- the interior of the helix -- and region (2) -- the dielectric layer adjacent to the exterior of the helix. See Eqs. (12), (17), and (23).

As a practical matter, the determinant in Eq. (39) must be truncated. The hope is that convergence is fast and that only a few terms are needed for good accuracy; this hope is realized below, in Section 4 where approximate roots of Eq.(39) are found numerically. Even the lowest order expansion (using a single Chebyshev polynomial in the expansions) can give good results; in this case the dispersion relation becomes

$$\det M_{00} = 0 \tag{40}$$

where

$$M_{00} = \sum_{n=-\infty}^{\infty} \begin{pmatrix} J_0(\alpha_n) & 0 \\ 0 & J_1(\alpha_n)/\alpha_n \end{pmatrix} \widetilde{Z}_n \begin{pmatrix} J_0(\alpha_n) & 0 \\ 0 & J_1(\alpha_n)/\alpha_n \end{pmatrix}. \tag{41}$$

In this case, the roots of a 2×2 determinant must be found.

To compare this result with previous work, consider the commonly made assumptions

$$J_\xi(s) = \text{constant (independent of } s\text{)}, \tag{42a}$$

$$J_\eta(s) = 0. \tag{42b}$$

In this case it is straightforward to show, from Eq.(29) that

$$E_\xi \simeq \frac{(w/2)J_\xi}{\pi a \sin \psi} \sum_n e^{-j\alpha_n s} \frac{\sin \alpha_n}{\alpha_n} \widetilde{Z}_n^{(1,1)} \tag{43}$$

where $\widetilde{Z}_n^{(1,1)}$ is the (1,1) element of $\widetilde{Z}_n$. A further approximation is commonly made in one of two ways. Either

12

$$E_\xi(s=0)=0 \quad (E_\xi \text{ vanishes on tape centerline}), \tag{44a}$$

or
$$\int_{-1}^{1} ds E_\xi(s)=0 \quad (\text{Average value of } E_\xi \text{ vanishes}). \tag{44b}$$

In these cases, using Eq.(43), the dispersion relation becomes

$$\sum_n \left(\frac{\sin\alpha_n}{\alpha_n}\right)^M \tilde{Z}_n^{(1,1)} = 0 \tag{45}$$

where $M=1$ for (44a), $M=2$ for (44b). Generally the choice of (44a) or (44b) makes very little difference to the computed values of phase velocity. Numerical solutions to Eq.(39), and comparisons with the solutions of (45) are given in Section 4. First the corresponding expression for the interaction impedance is derived.

Once (approximate) roots of Eq. (39) are found, these are used in Eq. (38) to find the current J. Once J_ξ and J_η are determined, the electric and magnetic fields then follow from Eqs. (29) and (11), after using Eq.(21) (inverted) to change back to (θ, z) coordinates, from (ξ, η). Finally, once the fields are known, the interaction impedance for the n-th spatial harmonic at radius r may be computed from its definition,

$$\mathsf{K}_n(r) \equiv \frac{|E_{zn}^{(1)}(r)|^2}{2\beta_n^2 P_r} \tag{46}$$

where P_r is the power flowing along the helix. P_r is given by the real part of

$$P = \tfrac{1}{2}\int \vec{E}\times\vec{H}*d\hat{a} = \pi \sum_{n=-\infty}^{\infty}\int_0^b rdr(E_{rn}H_{\theta n}^* - E_{\theta n}H_{rn}^*)$$

$$= \pi\omega\varepsilon_o \sum_{n=-\infty}^{\infty}\beta_n\int_o^b rdr\gamma_n^{-4}\left\{ \begin{array}{l} \varepsilon_r\left[\left|\frac{\partial}{\partial r}E_{zn}\right|^2 + \frac{n^2}{r^2}|E_{zn}|^2\right] + \zeta_o^2\left[\left|\frac{\partial}{\partial r}H_{zn}\right|^2 + \frac{n^2}{r^2}|H_{zn}|^2\right] \\ + j\zeta_o\frac{n}{r}\left[\varepsilon_r\frac{\omega}{\beta_n c}\frac{\partial}{\partial r}\left(E_{zn}^*H_{zn}\right) - \frac{\beta_n c}{\omega}\frac{\partial}{\partial r}\left(E_{zn}H_{zn}^*\right)\right] \end{array}\right\} \tag{47}$$

where the surface integral has been evaluated over a plane normal to the z-axis and we have used Eqs. (8a-d) to express all transverse field components in terms of axial components.

The integrals in Eq. (47) may all be carried out explicitly by using the indefinite integral

13

$$\int_0^x x' \mathfrak{J}_n^2(x')dx' = \frac{1}{2}\Big[(x^2 + n^2)\mathfrak{J}_n^2(x) - x^2 \mathfrak{J}_n'^2(x)\Big] \tag{48}$$

where $\mathfrak{J}_n(x)$ is any linear combination of the modified Bessel functions $I_n(x)$ and $K_n(x)$. The result for the power flowing in the nth spatial harmonic, in region *(i)*, *i=1,2*, is $P_n^{(i)}\big(a^{(i)}\big) - P_n^{(i)}\big(a^{(i-1)}\big)$ where

$$
\begin{aligned}
P_n^{(i)}(r) = \frac{\pi\omega\varepsilon_0\beta_n}{\gamma_n^{(i)4}} \Bigg\{ &\varepsilon_r^{(i)}\Big[rE_{zn}^* \tfrac{\partial}{\partial r} E_{zn} - \tfrac{1}{2}\big(\gamma_n^{(i)2}r^2 + n^2\big)|E_{zn}|^2 - \gamma_n^{(i)2}r^2\big|\tfrac{\partial}{\partial r} E_{zn}\big|^2 \Big] \\
&+ \zeta_0^2\Big[rH_{zn}^* \tfrac{\partial}{\partial r} H_{zn} - \tfrac{1}{2}\big(\gamma_n^{(i)2}r^2 + n^2\big)|H_{zn}|^2 - \gamma_n^{(i)2}r^2\big|\tfrac{\partial}{\partial r} H_{zn}\big|^2 \Big] \\
&+ jn\zeta_0\Big[\varepsilon_r^{(i)} \tfrac{\omega}{\beta_n c} E_{zn}^* H_{zn} - \tfrac{\beta_n c}{\omega} E_{zn}H_{zn}^*\Big]\Bigg\}
\end{aligned}
\tag{49}
$$

where $a^{(0)} \equiv 0, a^{(1)} \equiv a, a^{(2)} \equiv b$ and all fields in Eq. (49) are obtained from the current eigenvector $\mathfrak{J}$, as described above.

The total power flowing is then just

$$P = \sum_{i=1}^{2} \sum_{n=-\infty}^{\infty} P_n^{(i)} \tag{50}$$

When metallic vanes are present, an approximate model may be simply implemented; as shown in the Appendix.

3. Stratified Dielectric Supporting Layer

When the dielectric layer supporting the helix is stratified, as shown in Figure 2, the analysis following Eq. (15), up to and including the dispersion relation, Eq. (39), continues to hold if the admittance matrix of Eq. (12) is redefined, as shown below.
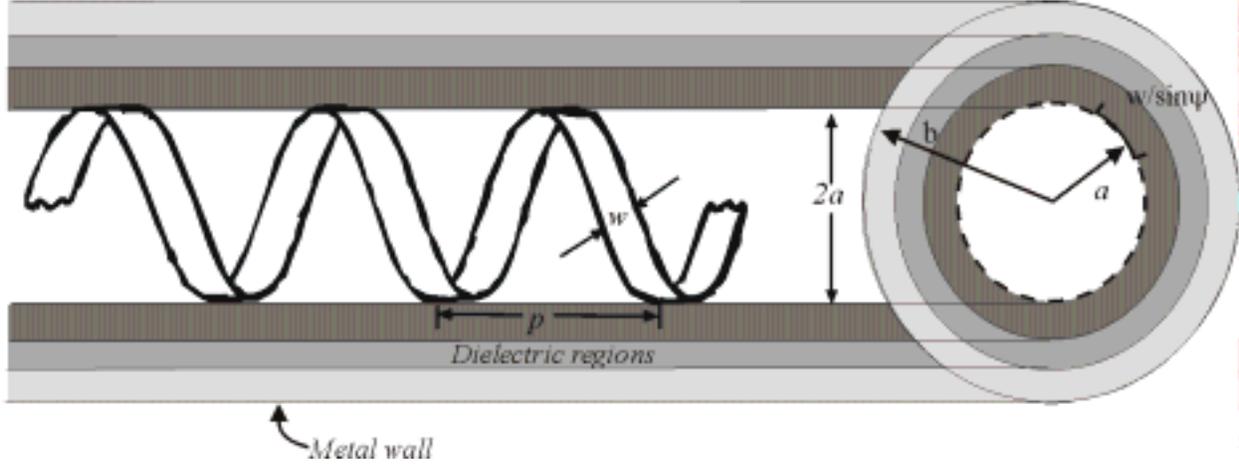
Figure 2: Tape helix supported by a stratified dielectric

The stratified case is important because it facilitates the analysis of arbitrarily shaped rods, as illustrated in Figure 3. It has been shown by Kory[12] and by Jain and Basu[13] that multiple azimuthally symmetric layers will represent different rod shapes to good accuracy if the values of the smoothed dielectric constants are assigned using area weighting, i.e.

$$\bar{\varepsilon}_r = 1 + (\varepsilon_r - 1)\frac{A}{A + A'} \tag{51}$$

in the case of Figure 3, where ε_r and A are the relative permittivity and cross sectional area of the rods respectively within the indicated annular layer, and $3(A + A') = \bar{A}$ is the cross sectional area of the smoothed layer in this case. See Figure 3.
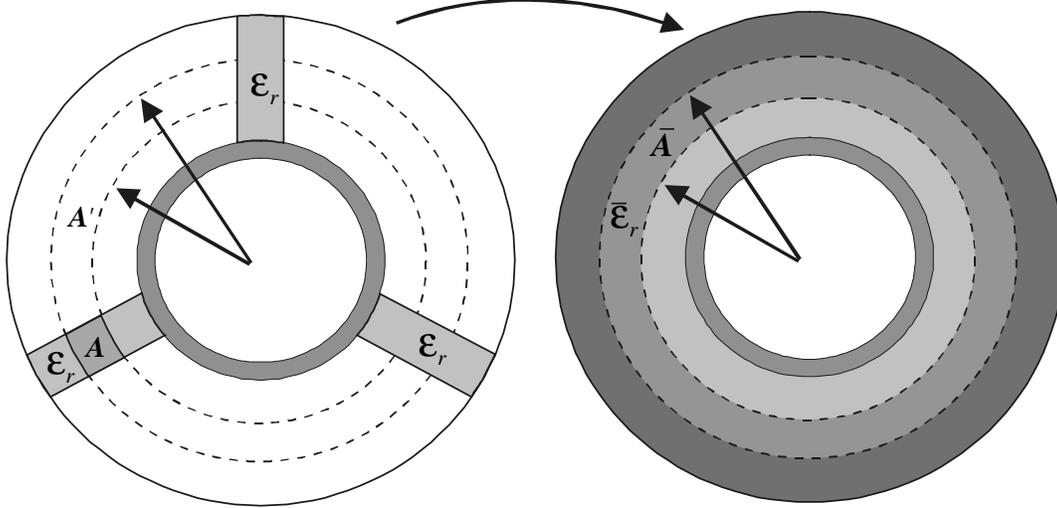
Figure 3: Use of multiple symmetric layers to represent arbitrary rod shape is reasonably accurate when the value of the smoothed dielectric constant is assigned according to Eq. (51).

We proceed to consider the case of N radial regions, as shown in Figure 4. Region 1 is, as before, the interior of the helix, assumed to be vacuum. Region 2 is the first dielectric layer outside the helix. Region N is the outermost dielectric layer, adjacent to the metal wall. The relative permittivity of region (i) is denoted $\varepsilon_r^{(i)}$; $r = a^{(1)} \equiv a$ is the helix radius, $r = a^{(i)}$ is the outer boundary of region (i), and $r = a^{(N)} = b$ is the radius of the outer wall.
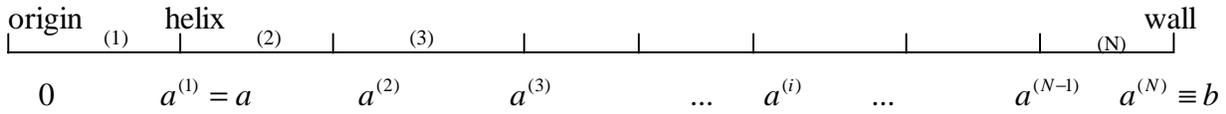
Figure 4: N region problem. Region 1 is the interior of the helix. Regions 2, 3, … N are dielectric supporting layers. The outer boundary of region (i) is at $r = a^{(i)}$.

The analysis begins by noting that application of the continuity conditions on the parallel components of $\vec{E}$ and $\vec{H}$ at the interface between two dielectric layers will generally couple the parallel $\vec{E}$ and $\vec{H}$ fields. We therefore anticipate in particular the existence of relations of the form

$$\frac{\partial}{\partial r} E_{zn}^{(i)} = \gamma_n^{(i)} \left[l_{EEn}^{(i)} E_{zn}^{(i)} + \zeta_o l_{EHn}^{(i)} jH_{zn}^{(i)} \right] \tag{52a}$$

$$j\frac{\partial}{\partial r} H_{zn}^{(i)} = \gamma_n^{(i)} \left[\zeta_o^{-1} l_{HEn}^{(i)} E_{zn}^{(i)} + l_{HHn}^{(i)} jH_{zn}^{(i)} \right] \tag{52b}$$

at $r = a^{(1)} \equiv a$ for regions 1 and 2 ($i=1,2$, adjacent to the helix), where the coefficients $l_{EEn}^{(i)}, l_{EHn,}^{(i)} l_{HEn}^{(i)}$ and $l_{HHn}^{(i)}$ are to be determined from the field equations and boundary conditions at the outer metallic wall. Equations (52a,b) are generalizations of Eqs (10a,b). Substituting (52a,b) in Eqs. (8b,d) and solving for $H_{\theta n}$ and H_{zn} in terms of $E_{\theta n}$ and E_{zn} again gives a relation of the form Eq. (11) above, where the admittance matrix is now given by

$$
Y_n^{(i)} = \frac{-j\beta_n c}{\zeta_o \gamma_n^{(i)} \omega a l_{HHn}^{(i)}}
$$

$$
\begin{pmatrix}
n + \dfrac{\omega \varepsilon_r^{(i)} \gamma_n^{(i)} a}{\beta_n c} l_{EHn}^{(i)} & \dfrac{\beta_n}{\gamma_n^{(i)2} a}(n + \dfrac{\omega \varepsilon_r^{(i)} \gamma_n^{(i)} a}{\beta_n c} l_{EHn}^{(i)})(n + \dfrac{\omega \gamma_n^{(i)} a}{\beta_n c} l_{HEn}^{(i)}) - \varepsilon_r^{(i)} \dfrac{\omega^2}{c^2} \dfrac{a}{\beta_n} l_{HHn}^{(i)} l_{EEn}^{(i)} \\
-\dfrac{\gamma_n^{(i)2} a}{\beta_n} & -n - \dfrac{\omega \gamma_n^{(i)} a}{\beta_n c} l_{HEn}^{(i)}
\end{pmatrix} (53)
$$

It remains only to specify values for $l_{EEn}^{(i)}, l_{EHn}^{(i)}, l_{HEn}^{(i)}$ and $l_{HHn}^{(i)}$ in regions 1 and 2, for use in Eq. (53). In region 1 there is no coupling between the E and H fields; the coefficients therefore are the same as for the single layer case, i.e.

$$
l_{EEn}^{(1)} = l_{En}^{(1)}, \tag{54a}
$$

$$
l_{EHn}^{(1)} = l_{HEn}^{(1)} = 0, \tag{54b}
$$

$$
l_{HHn}^{(1)} = l_{Hn}^{(1)}, \tag{54c}
$$

where $l_{En}^{(1)}$ and $l_{Hn}^{(1)}$ are given in Eq.(13).

To calculate the coefficients $l_{EEn}^{(2)}$, etc. in region 2, the basic idea is to use the field equations to "propagate" the E_z and H_z fields from the helix surface, through the dielectric layers, to the outer wall where the boundary conditions are applied.

Using solutions of Eq. (5), it is straightforward to show that within a layer (region (i), say), the E_z field at r_2 is related to the E_z field at r_1 by

$$\begin{pmatrix} E_{zn}^{(i)}(r_2) \\ \gamma_n^{(i)^{-1}} \frac{\partial}{\partial r} E_{zn}^{(i)}(r_2) \end{pmatrix} =$$

$$x_{n1}^{(i)} \begin{pmatrix} -I_n(x_{n2}^{(i)})K_n'(x_{n1}^{(i)}) + I_n'(x_{n1}^{(i)})K_n(x_{n2}^{(i)}) & I_n(x_{n2}^{(i)})K_n(x_{n1}^{(i)}) - I_n(x_{n1}^{(i)})K_n(x_{n2}^{(i)}) \\ -I_n'(x_{n2}^{(i)})K_n'(x_{n1}^{(i)}) + I_n'(x_{n1}^{(i)})K_n'(x_{n2}^{(i)}) & I_n'(x_{n2}^{(i)})K_n(x_{n1}^{(i)}) - I_n(x_{n1}^{(i)})K_n'(x_{n2}^{(i)}) \end{pmatrix} \begin{pmatrix} E_{zn}^{(i)}(r_1) \\ \gamma_n^{(i)^{-1}} \frac{\partial}{\partial r} E_{zn}^{(i)}(r_1) \end{pmatrix}$$

$$\equiv U_n^{(i)}(r_2|r_1) \begin{pmatrix} E_{zn}^{(i)}(r_1) \\ \gamma_n^{(i)^{-1}} \frac{\partial}{\partial r} E_{zn}^{(i)}(r_1) \end{pmatrix} \tag{55}$$

where $x_{n1}^{(i)} \equiv \gamma_n^{(i)} r_1$, $x_{n2}^{(i)} \equiv \gamma_n^{(i)} r_2$, and where we have defined the propagation matrix $U_n^{(i)}(r_2|r_1)$ for region *(i)*.

Since $H_{zn}^{(i)}(r)$ satisfies the same equation (Eq. (5)) as $E_{zn}^{(i)}$ its propagation matrix in region *(i)* is also $U^{(i)}(r_2|r_1)$. Defining then the 4-component vector

$$V_n^{(i)}(r) \equiv \begin{pmatrix} E_{zn}^{(i)}(r) \\ \gamma_n^{(i)^{-1}} \frac{\partial}{\partial r} E_{zn}^{(i)}(r) \\ j\, H_{zn}^{(i)}(r) \\ \gamma_n^{(i)^{-1}} j \frac{\partial}{\partial r} H_{zn}^{(i)}(r) \end{pmatrix} \tag{56}$$

we therefore have

$$V_n^{(i)}(r_2) = W_n^{(i)}(r_2|r_1) V_n^{(i)}(r_1) \tag{57}$$

where $W_n^{(i)}(r_2|r_1)$ is the 4×4 matrix,

$$W_n^{(i)}(r_2|r_1) \equiv \begin{pmatrix} U_n^{(i)}(r_2|r_1) & 0 \\ 0 & U_n^{(i)}(r_2|r_1) \end{pmatrix}. \tag{58}$$

Next we evaluate the jump conditions across a boundary separating two regions, say regions *(i)* and *(i+1)*. Refer to Figure 5.
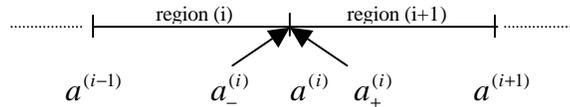
Figure 5: Radial regions *(i)* and *(i+1)* and their common boundary at $r = a^{(i)}$.

Denote by $a_-^{(i)}$ the location adjacent to $a^{(i)}$ just inside region *(i)*. Similarly, denote by $a_+^{(i)}$ the location adjacent to $a^{(i)}$, just inside region *(i+1)*. Then using Eq. (8b) and Eq. (8d) and enforcing continuity of $E_{\theta n}$ and $H_{\theta n}$, it follows that

$$V_n^{(i+1)}(a_+^{(i)}) = T_n(a_+^{(i)} \mid a_-^{(i)})V_n^{(i)}(a_-^{(i)}) \tag{59}$$

where

$$T_n(a_+^{(i)} \mid a_-^{(i)}) \equiv \begin{pmatrix} 1 & 0 & 0 & 0 \\ 0 & \dfrac{\varepsilon_r^{(i)}}{\varepsilon_r^{(i+1)}}\dfrac{\gamma_n^{(i+1)}}{\gamma_n^{(i)}} & F_n^{(i)} & 0 \\ 0 & 0 & 1 & 0 \\ \varepsilon_r^{(i+1)}F_n^{(i)}/\zeta_o^2 & 0 & 0 & \dfrac{\gamma_n^{(i+1)}}{\gamma_n^{(i)}} \end{pmatrix} \tag{60}$$

$$F_n^{(i)} \equiv \zeta_0 \frac{\omega n \beta_n}{a^{(i)}c} \frac{1}{\gamma_n^{(i+1)}\gamma_n^{(i)2}} \frac{\varepsilon_r^{(i)} - \varepsilon_r^{(i+1)}}{\varepsilon_r^{(i+1)}}. \tag{61}$$

We now have all the ingredients needed to propagate the vector V_n from the helix at $r = a \equiv a_+^{(1)}$ to the outer wall, at $r = b \equiv a_-^{(N)}$:

$$V_n^{(N)}(b) = W_n(b \mid a_+^{(N-1)}) \cdot T_n(a_+^{(N-1)} \mid a_-^{(N-1)}) \dots T_n(a_+^{(2)} \mid a_-^{(2)})W_n(a_-^{(2)} \mid a)V_n^{(2)}(a)$$
$$\equiv S(b \mid a)V_n^{(2)}(a), \tag{62}$$

which defines the 4×4 matrix *S(b/a)* that propagates the vector V_n from the helix to the outer wall. It is clear that *S(b/a)* may be simply constructed numerically in any specific case by performing the matrix multiplications indicated in Eq. (62).

The boundary conditions at *r=b* are

$$E_{zn}(b) = 0 \tag{63a}$$

$$\tfrac{\partial}{\partial r}B_{zn}(b) = 0 \tag{63b}$$

which means that the first and fourth elements of $V_n^{(N)}(b)$ in Eq. (63) vanish. Writing out the first and fourth rows of (62) yields

$$S_{11}E_{zn}^{(2)} + S_{12}\gamma_n^{(2)^{-1}} \tfrac{\partial}{\partial r}E_{zn}^{(2)} + S_{13}jH_{zn}^{(2)} + S_{14}\gamma_n^{(2)^{-1}}j\tfrac{\partial}{\partial r}H_{zn}^{(2)} = 0 \tag{64a}$$

$$S_{41}E_{zn}^{(2)} + S_{42}\gamma_n^{(2)^{-1}} \tfrac{\partial}{\partial r}E_{zn}^{(2)} + S_{43}jH_{zn}^{(2)} + S_{44}\gamma_n^{(2)^{-1}}j\tfrac{\partial}{\partial r}H_{zn}^{(2)} = 0 \tag{64b}$$

Solving these equations for $\tfrac{\partial}{\partial r}E_{zn}^{(2)}$ and $\tfrac{\partial}{\partial r}H_{zn}^{(2)}$ in terms of $E_{zn}^{(2)}$ and $H_{zn}^{(2)}$ then gives relations of precisely the form (52a,b) where

$$l_{EEn}^{(2)} = \frac{1}{D}(S_{44}S_{11} - S_{14}S_{41}) \tag{65a}$$

$$l_{EHn}^{(2)} = \frac{1}{\zeta_o D}(S_{44}S_{13} - S_{14}S_{43}) \tag{65b}$$

$$l_{HEn}^{(2)} = \frac{\zeta_o}{D}(-S_{42}S_{11} + S_{12}S_{41}) \tag{65c}$$

$$l_{HHn}^{(2)} = \frac{1}{D}(-S_{42}S_{13} + S_{12}S_{43}) \tag{65d}$$

and $D \equiv S_{14}S_{42} - S_{12}S_{44}$. Use of these values in the admittance matrix of Eq. (53) will lead to the correct dispersion relation for a helix supported by the stratified dielectric layer of Figure 4.

The interaction impedance for the multi-layer case may be computed from the power flow, as defined in Eq.(46). The power flowing in region (i) in spatial harmonic n is still given by Eq.(49). The total power is given by Eq.(50), where the sum on regions (i) is now extended from 1 to N.

4. Numerical Results and Discussion

A FORTRAN function `dtape` has been written to evaluate det M in Eq. (39) for specified values of ω, β, and other parameters. The matrix M is truncated at a user-specified value of the maximum order (l_{max})of Chebyshev polynomial to be used in the expansions of the currents, Eq.(33a,b). Each matrix element is evaluated by including terms up to a user-specified maximum spatial harmonic number[14] ($\pm n_{max}$) in Eq. (37). `dtape` also evaluates, for special values of one of its arguments, the approximate dispersion function on the left hand side of Eq.(45), if needed for comparison purposes; this feature has been used in preparing the comparison plots, below.

A FORTRAN subroutine `ktape` has also been written to compute the interaction impedance (46), using the approach described in Section 2.

20

Finally, a FORTRAN program, `droot`, has been written to find a root of `dtape` using Newton's method, and to call `ktape`[15].

As an example, we consider a tape helix supported by a single dielectric layer with parameters shown in Table 1.

Table 1
Tape helix parameters used in examples

Parameter	Value
Tape radius (a)	0.1245 cm
Pitch (p)	0.0801 cm
Helix pitch angle (ψ)	5.85°
Wall radius (b)	0.2794 cm
Dielectric constant of supporting layer ($\varepsilon_r^{(2)}$)	1.25

Two different tape widths, one narrow ($\overline{w} = 0.2$) and one wide ($\overline{w} = 0.8$), are used to make the phase velocity and impedance vs. frequency plots shown below. Two different approximations are used to produce the results shown in each plot. These are (I) truncated Chebyshev expansion of the currents, with $l_{max} = 4$ and $n_{max} = 24$, and (II) constant longitudinal helix current, zero transverse current, and longitudinal $E = 0$ on tape centerline [Re: Eq.(45), with $M=1$ and $n_{max} = 24$]. (The use of Eq.(45) with $M=2$ produced plots in all cases indistinguishable from those using $M=1$.) In all cases, 24 spatial harmonics are retained in the sums; though this may seem excessive, we find this to be required to obtain reasonably good representations of the tape currents (See Figures 7 and 9, below). Use of $l_{max} = 2$ and $n_{max} = 12$ gives results for phase velocity and impedance (but not currents!) that agree to three or four digits with those obtained using the higher order expansions. With $l_{max} = 4$ and $n_{max} = 24$, the computation of phase velocity and impedance at 51 equally spaced frequencies takes about 24 seconds on an HP-9000/780 workstation; all computations are done in double precision.

Figures 6a and 6b show, respectively, the phase velocity and (on-axis) interaction impedance as functions of frequency for a narrow tape, with normalized tape width $\overline{w} \equiv w/(p \cos \psi) = 0.2$.

The plots show that, as expected for a narrow tape, there is a very small error made using Approximation (II).

Figure 7 shows the longitudinal ($J_\xi(s)$) and transverse ($J_\eta(s)$) surface currents on the tape for this case. The transverse current is extremely small, as expected, and the longitudinal current is quite flat across the tape, except very near the edge singularities.

In Figures 8a,b the phase velocity and impedance plots are shown for a wide tape, with a normalized tape width of 0.8. Here we see that the use of the Chebyshev expansion makes a significant difference, both to the phase velocity and to the interaction impedance, when compared to the values obtained using the assumption of a constant longitudinal current and zero transverse current on the tape. Figure 9 shows the helix surface currents in this case. Note that while the transverse current is still small, it is much larger (relative to the longitudinal current) than that in Figure 7. The longitudinal current shows a large variation across the tape in this case, and is highly asymmetric about the tape centerline.
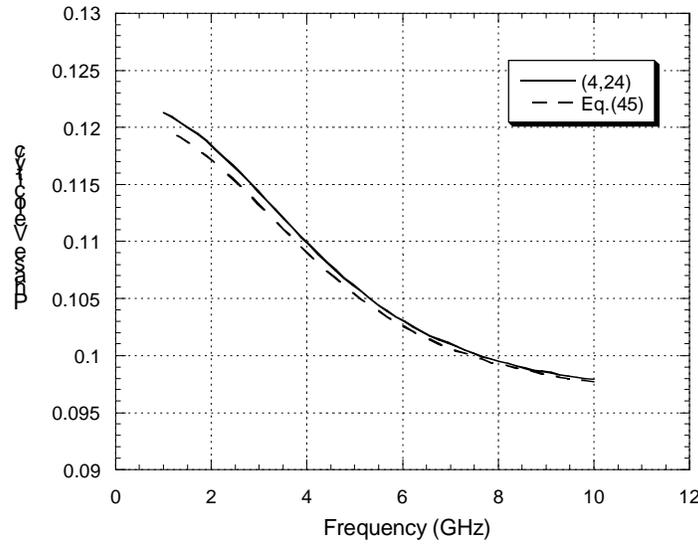
Figure 6a: Phase velocity vs. frequency for a narrow tape helix with the parameters of Table 1 and *w/pcosψ = 0.2* as computed using (1) the Chebyshev expansion with (1_{max}=4; n_{max}=24) [solid line], and (2) the assumptions that the longitudinal current on the tape is constant, the transverse current is zero, and the parallel electric field along the helix centerline vanishes (Eq. (45), *M=1*; n_{max}=24) [dashed line].
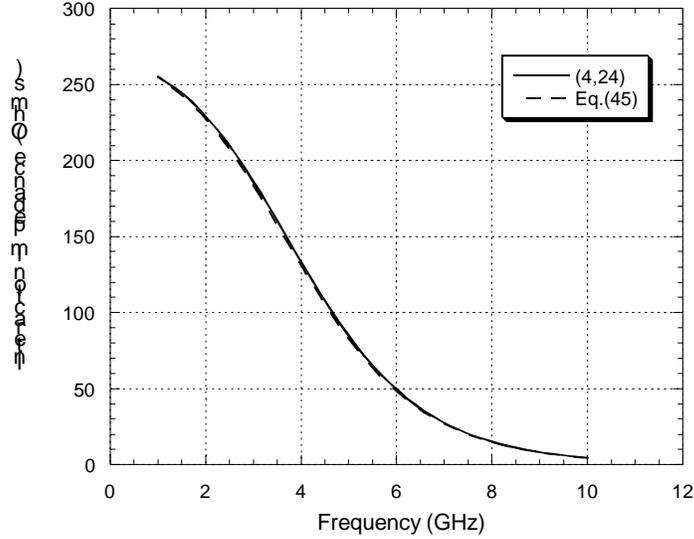
Figure 6b: On-axis interaction impedance vs. frequency for a narrow tape helix with the parameters of Table 1 and $w/pcos\psi = 0.2$ as computed using (1) the Chebyshev expansion with ($l_{max}=4$; $n_{max}=24$) [solid line], and (2) the assumptions that the longitudinal current on the tape is constant, the transverse current is zero, and the parallel electric field along the helix centerline vanishes (Eq. (45), $M=1$; $n_{max}=24$) [dashed line].
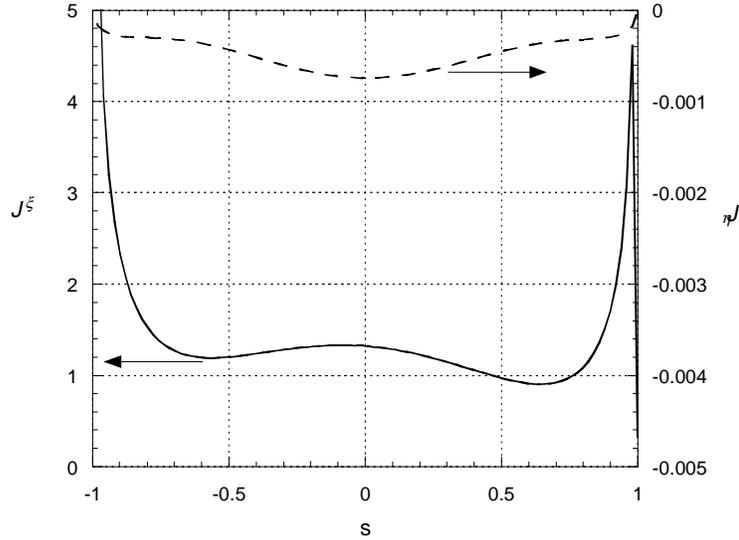
Figure 7: Longitudinal and transverse currents vs. s for a narrow tape helix with the parameters of Table 1 and $w/pcos\psi = 0.2$ as computed using the Chebyshev expansion with ($l_{max}=4$; $n_{max}=24$). The units have been fixed by setting $J_{\xi 0} = 1$ in Eq.(33a).
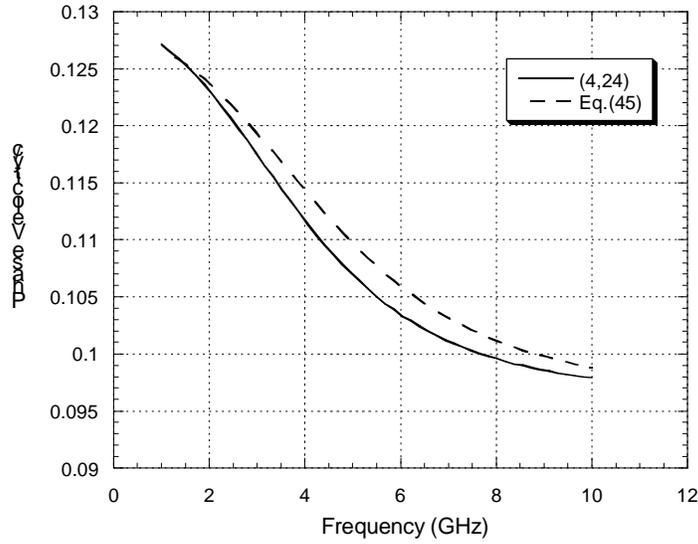
Figure 8a: Phase velocity vs. frequency for a wide tape helix with the parameters of Table 1 and *w/pcosψ = 0.8* as computed using (1) the Chebyshev expansion with ($l_{max}=4$; $n_{max}=24$) [solid line], and (2) the assumptions that the longitudinal current on the tape is constant, the transverse current is zero, and the parallel electric field along the helix centerline vanishes (Eq. (45), *M=1*; $n_{max}=24$) [dashed line].
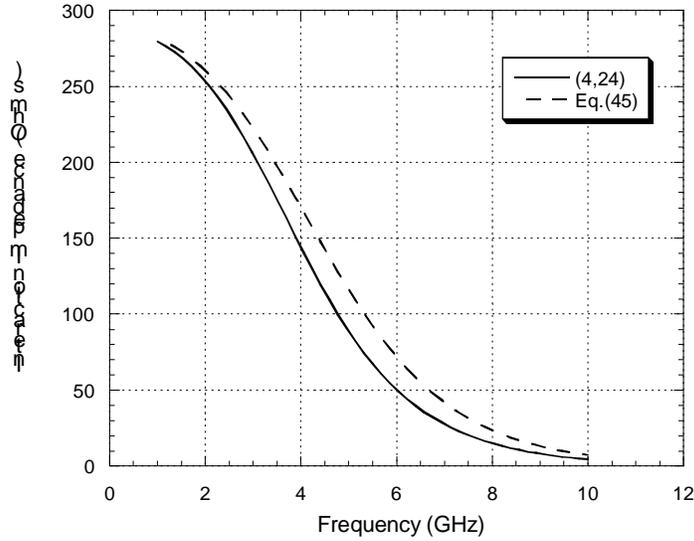
Figure 8b: On-axis interaction impedance vs. frequency for a wide tape helix with the parameters of Table 1 and *w/pcosψ = 0.8* as computed using (1) the Chebyshev expansion with ($l_{max}=4$; $n_{max}=24$) [solid line], and (2) the assumptions that the longitudinal current on the tape is constant, the transverse current is zero, and the parallel electric field along the helix centerline vanishes (Eq. (45), *M=1*; $n_{max}=24$) [dashed line].

24
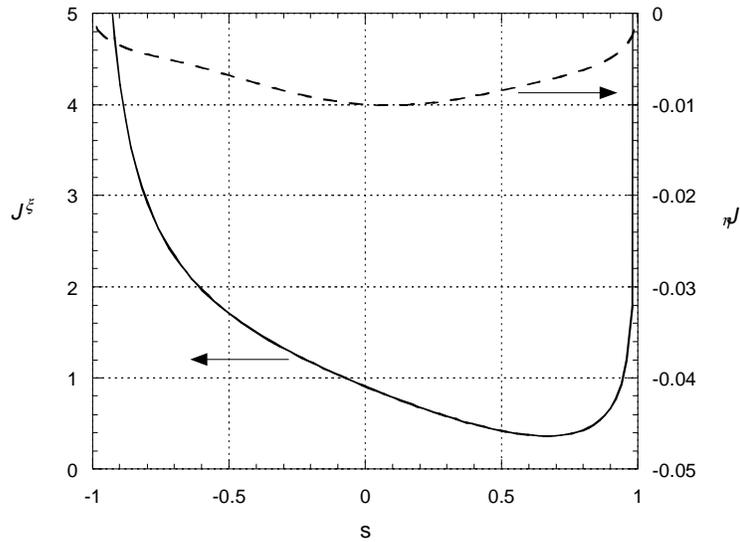
Figure 9: Longitudinal and transverse currents vs. *s* for a wide tape helix with the parameters of Table 1 and *w/pcosψ = 0.8* as computed using the Chebyshev expansion with ($l_{max}=4$; $n_{max}=24$). The units have been fixed by setting $J_{\xi 0} = 1$ in Eq.(33a). Note the *x10* scale on the right, compared to Figure 7.

If the interaction impedance (computed using the truncated Chebyshev expansion) is plotted versus normalized tape width, $\overline{w}$, for various frequencies, it is found that an optimum width exists, at which the impedance is maximized. An example is shown in Figure 10. Note that the maxima occur in this case near values of normalized tape width where neither the narrow tape nor narrow gap approximations would be expected to be accurate. The width at which the maximum impedance occurs increases as frequency decreases; the maxima are found to occur at a width that minimizes the phase velocity.
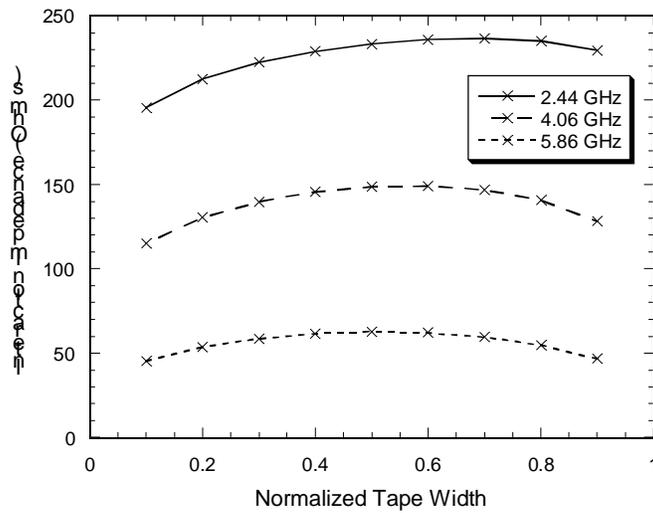
Figure 10: On-axis interaction impedance vs. normalized tape width for *f = 2.44, 4.06, and 5.86 GHz*, for a helix with the parameters of Table 1.

Acknowledgements

Appendix

Incorporation of a Simple Model of Vanes

Thin metal strips or wedges called vanes are sometimes used in helix TWT's to reduce circuit dispersion. The vanes are located adjacent to the dielectric support rods as shown in Figure A-1.
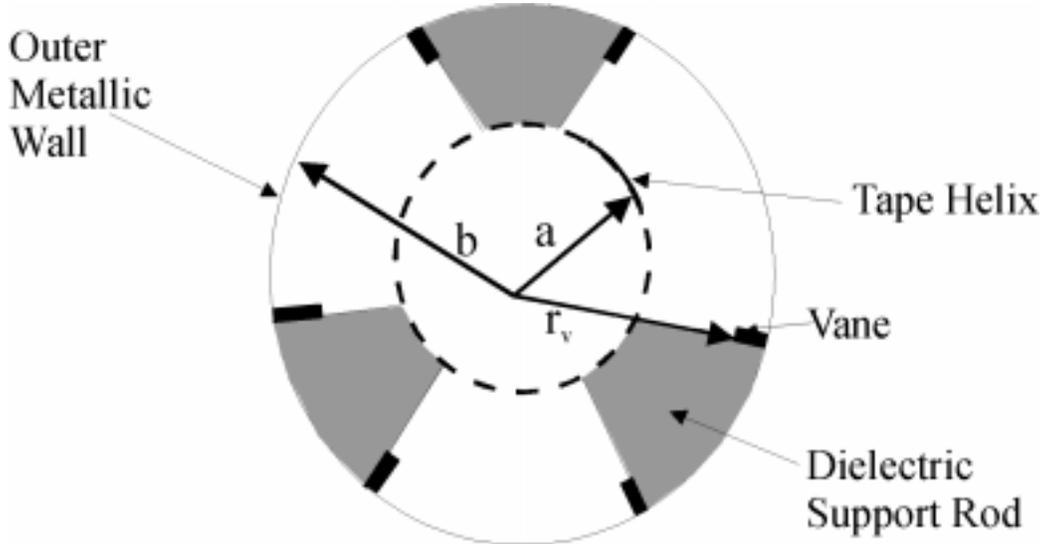
Figure A-1: Schematic of helix TWT cross-section, showing locations of metallic vanes.

Vanes tend to short out the E_z field while having little effect on E_θ or H_z. A simple model of the vanes has been published by Freund, et. al.[16] It effectively assumes that an infinite number of infinitely thin radial vanes are present. This model may be implemented by setting

$$E_z(r_v) = 0 \qquad\qquad (A\text{-}1)$$

where r_v is the radius of the vane tips, and

$$E_\theta(b) = 0 \qquad\qquad (A\text{-}2)$$

as before. These boundary conditions are easily incorporated into the calculation of the main text, by replacing $y_n^{(2)}$ in Eq.(14a) by $\gamma_n^{(2)} r_v$ and by the appropriate changes in the upper limit of integration in Eq.(47). Note that this is only an *approximate* model of the vanes. The dispersion and impedance calculations presented in the text, however, are *exact* when no vanes are present.

An example of the effects of vanes is illustrated in Figures A-2a and A-2b where the phase velocity and interaction impedance, respectively, are plotted versus frequency for a case with and

without vanes. Note the large reduction of dispersion comes with a cost in interaction impedance, due to the reduced value of E_z.
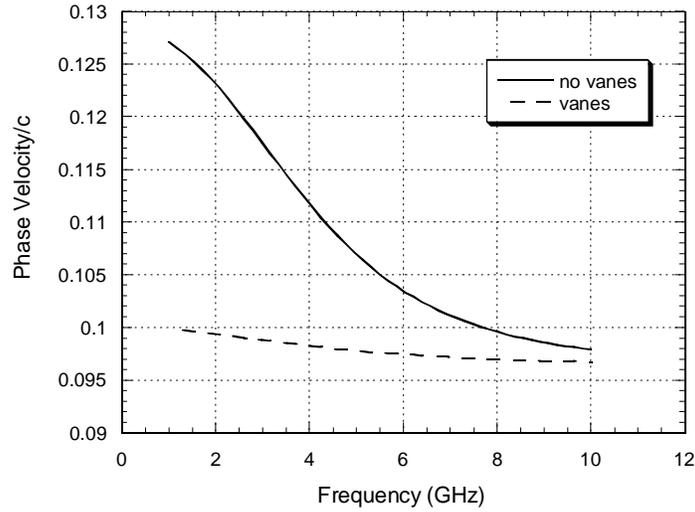
Figure A-2a: Phase velocity vs. frequency for a helix TWT circuit using the tape helix with the parameters of Table 1 and $w/pcos\psi = 0.8$ as computed using the Chebyshev expansion with $(1_{max}=4; n_{max}=24)$. with and without vanes. When vanes are present, $r_v = 0.2019$ cm.
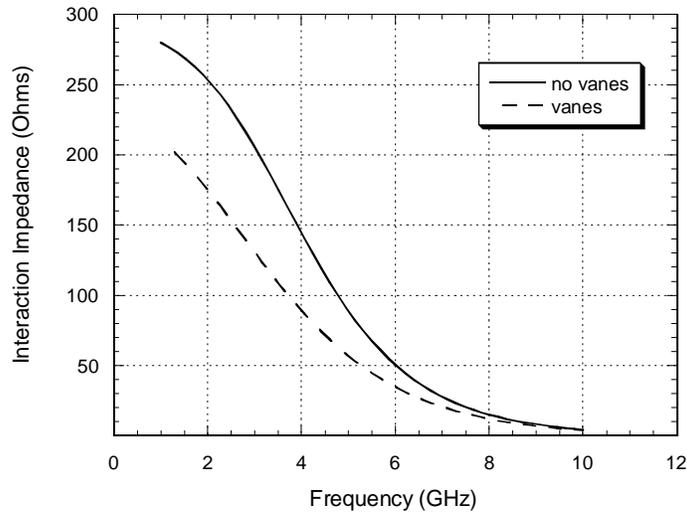
Figure A-2b: On-axis interaction impedance vs. frequency for same parameters as Figure A-2a.

References

[1] H.C. Pocklington, "Electrical oscillations in wires," Proc. Camb. Phil. Soc, **9** 324 (1897).

[2] R. Kompfner, *The Invention of the Traveling-Wave Tube*, San Francisco Press, 1963.

[3] J.R. Pierce, *Traveling Wave Tubes*, Van Nostrand, Princeton, NJ, 1950.

[4] S. Sensiper, "Electromagnetic wave propagation on helical conductors," Sc.D. thesis, Dept. of Electrical Engineering, MIT, May 1951.

[5] S. Sensiper, "Electromagnetic wave propagation on helical structures (A Review and survey of recent progress)," Proc IRE, **43** 149-161 (1955).

[6] P.K. Tien, "Traveling wave tube helix impedance," Proc IRE, **41** 1617-1623 (1953).

[7] J.B. McMurtry, "Fundamental interaction impedance of a helix surrounded by a dielectric and a metal shield," IRE Trans. Electron Dev, **ED-9** 210-216 (1962).

[8] D.A. Watkins, *Topics in Electromagnetic Theory*, J. Wiley, New York, 1958.

[9] H.P. Freund, N.R. Vanderplaats, and M.A. Kodis, "Field theory of a traveling wave tube amplifier with a tape helix," IEEE Trans. Plasma Sci. **21** 654-668 (1993).

[10] S. Ghosh, P.K. Jain, and B.N. Basu, "Rigorous tape analysis of inhomogeneously-loaded helical slow wave structures," IEEE Trans. Electron Dev. **44** 1158-1168 (1997).

[11] M. Abramowitz and I. Stegun, "Handbook of Mathematical Functions," Dover Publications, New York (1968) pp. 774ff.

[12] C.L. Kory, "Validation of an Accurate Three-Dimensional Helical Slow-Wave Circuit Model," NASA Contractor Report CR-4766 (1997).

[13] P.K. Jain and B.N. Basu, "The inhomogeneous dielectric loading effects of practical helix supports on the interaction impedance of the slow-wave structure of a TWT," IEEE Trans. Elect. Dev. **39** 727-733 (1992).

[14] Care must be taken to choose a sufficiently large cutoff to ensure convergence of the sum in Eq.(37). Generally, the maximum value of n should satisfy $\alpha_{n_{max}} \gg \left(\max(l,l')\right)^2 / 2$, so the Bessel functions in Eq..(37) are of order $O(n^{-1/2})$. Referring to the definition of α_n (Eq.(30)), this means that narrow tapes (small $\overline{w}$) require the retention of more spatial harmonics than wide tapes ($\overline{w}$ near 1). For sufficiently large values of n, it may be shown that all elements in the summand of Eq.(37) are of order $O(n^{-2})$.

[15] Electronic copies of `dtape`, `droot`, and `ktape` are available from one of the authors, subject to approval by NRL. Contact: *chernin@apo.saic.com.*

[16] H.P. Freund, E.G. Zaidman, and T.M. Antonsen, Jr., "Theory of helix traveling wave tubes with dielectric and vane loading", Phys. Plasmas, **3** 3146-3161 (1996).